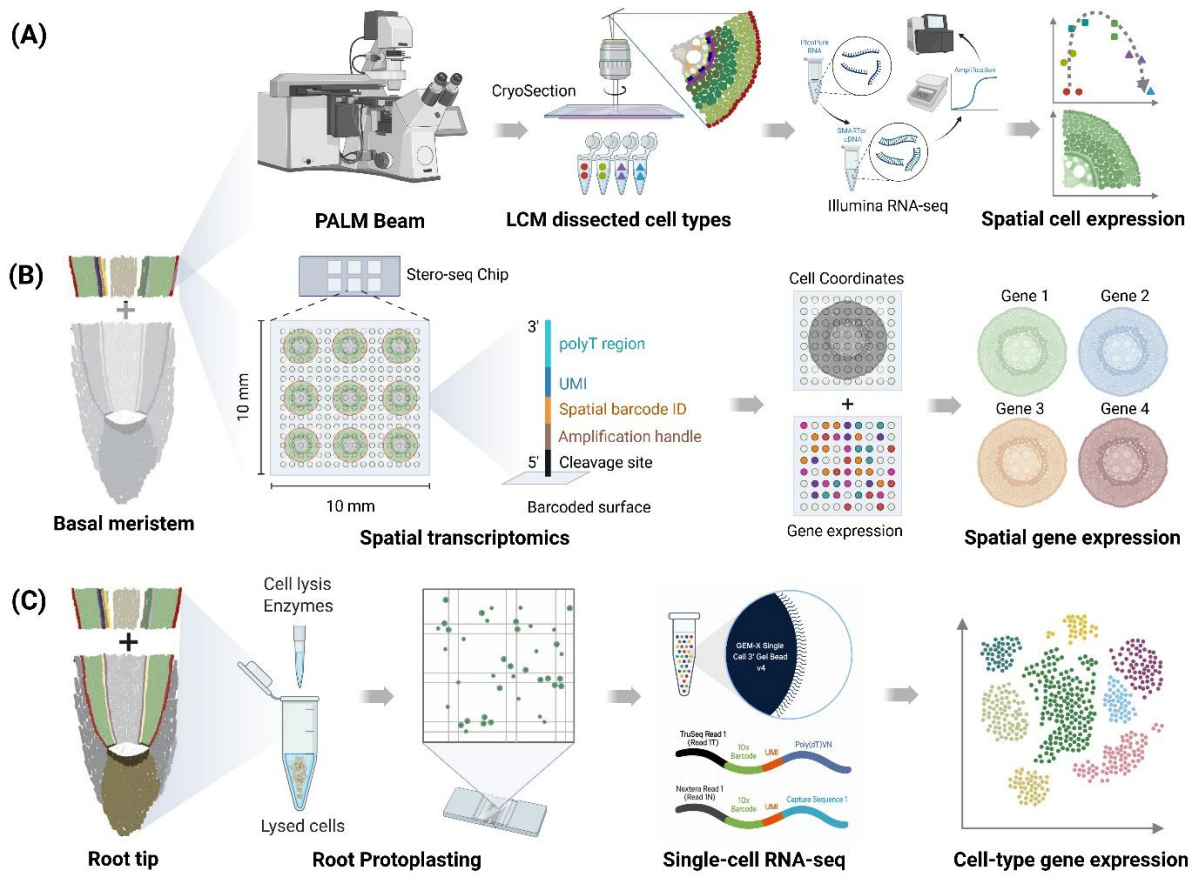
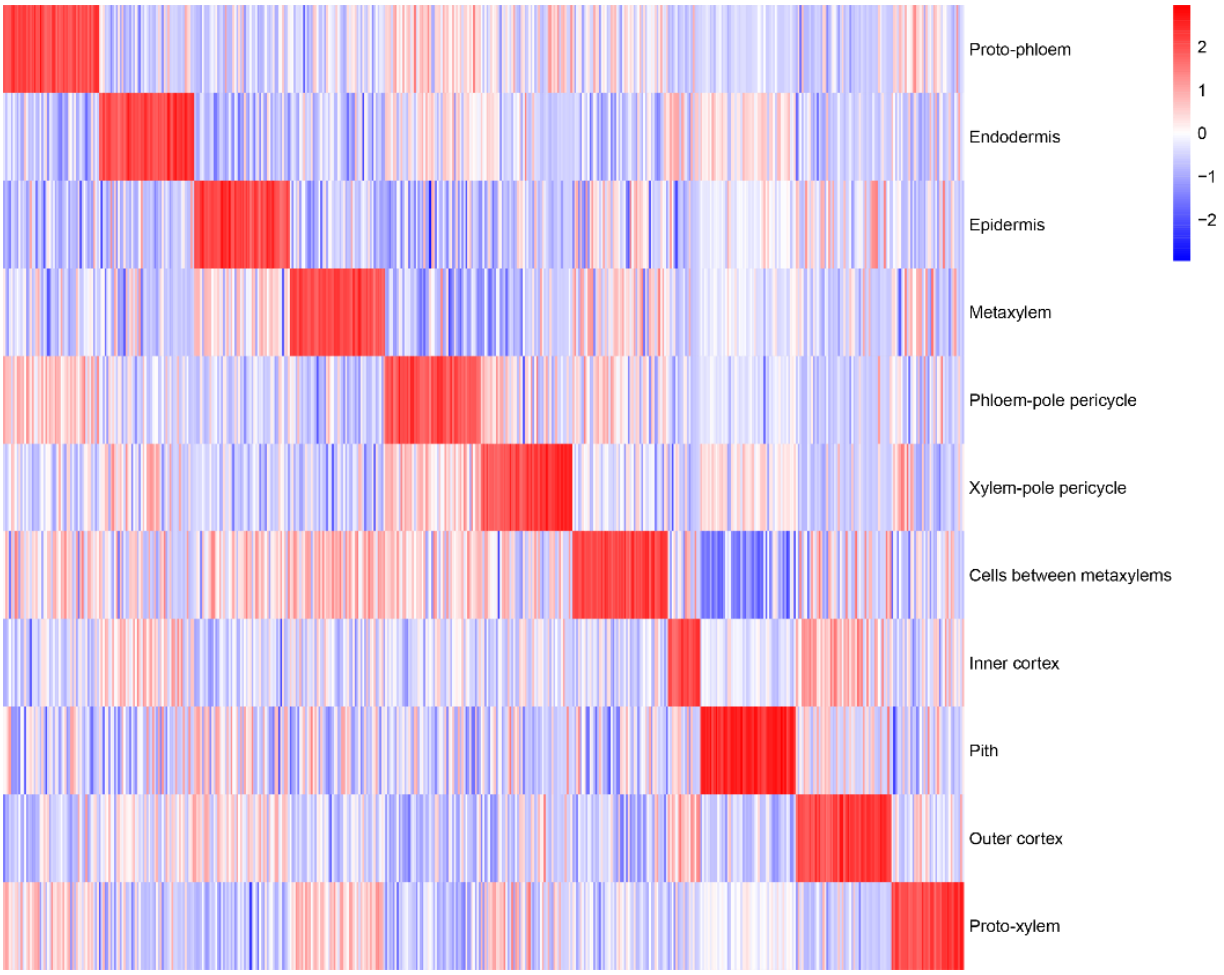
## Supplementary figures 1-24



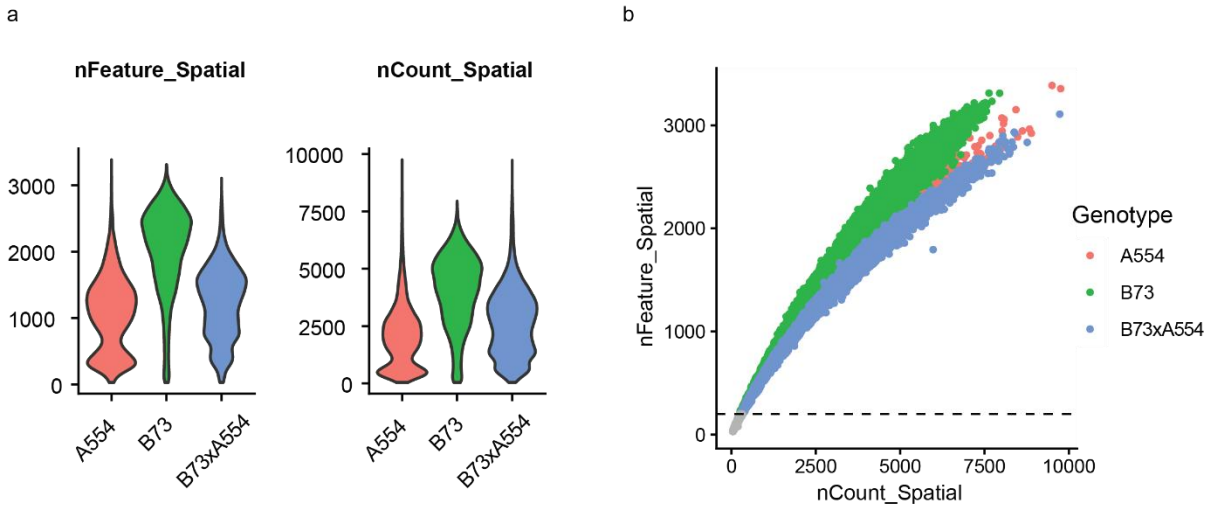

**Supplementary Figure 1. Complementary transcriptomic strategies for resolving cell-type and spatial gene expression in maize roots.**

(**A**) Laser-capture microdissection (LCM)-based cell-type transcriptomics. Maize root tissues are cryosectioned, and defined cell types or anatomical domains are isolated using a PALM laser microdissection system. RNA from the dissected material is processed for Illumina RNA sequencing, enabling cell-type-specific transcriptional profiling and reconstruction of gene-expression patterns across the root. (**B**) Spatial transcriptomics of the maize root basal meristem. Root cryosections are placed onto a spatially barcoded Stereo-seq chip, where transcripts are captured by oligonucleotides containing spatial barcode IDs, unique molecular identifiers (UMIs), and poly(T) sequences. Integration of transcript abundance with spatial coordinates enables reconstruction of the spatial distribution of individual genes across root tissues. (**C**) Single-cell RNA sequencing based on root protoplasting. Maize root tips are enzymatically digested to release individual protoplasts, which are subsequently captured and barcoded using the GEM-X single-cell platform before library preparation and sequencing. Transcriptomic profiles of individual cells are then used for dimensionality reduction, cell clustering, cell-type identification, and characterization of cell-type-specific gene expression.

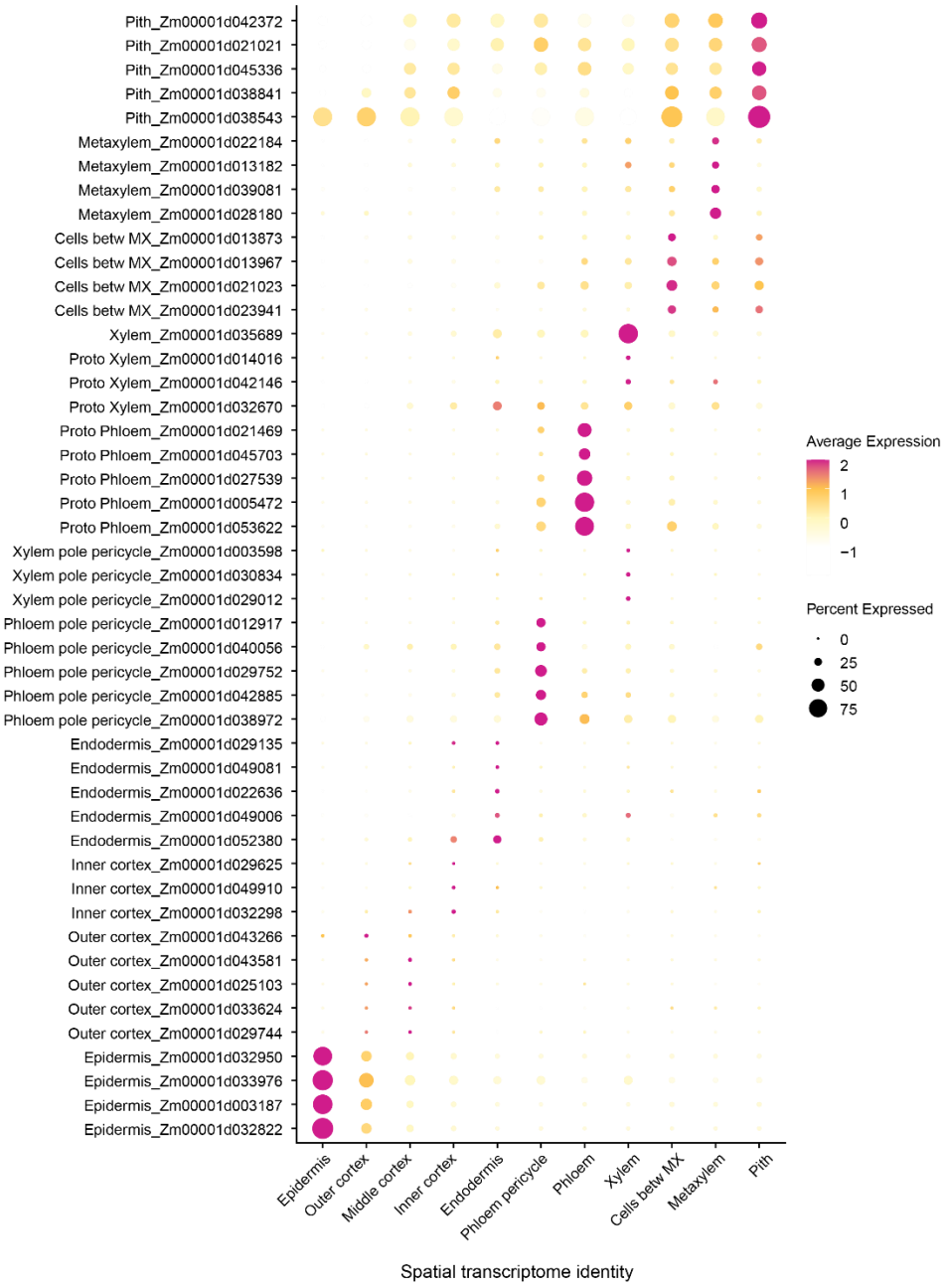



**Supplementary Figure S2. LCM-derived reference marker genes for maize root cell-type annotation.**

Heatmap showing the top 50 differentially expressed genes identified for each laser-capture microdissected (LCM) tissue or cell population by comparing one LCM sample with all other LCM samples. Rows represent the LCM-defined tissues, and columns represent the union of tissue-enriched marker genes, grouped according to their source tissue. Colours indicate standardized gene-expression levels, with red representing higher and blue representing lower relative expression. The tissue-enriched expression blocks demonstrate the specificity of the LCM reference profiles. These LCM-derived profiles were used as reference markers for annotating spatial transcriptomic and single-cell RNA-sequencing datasets.

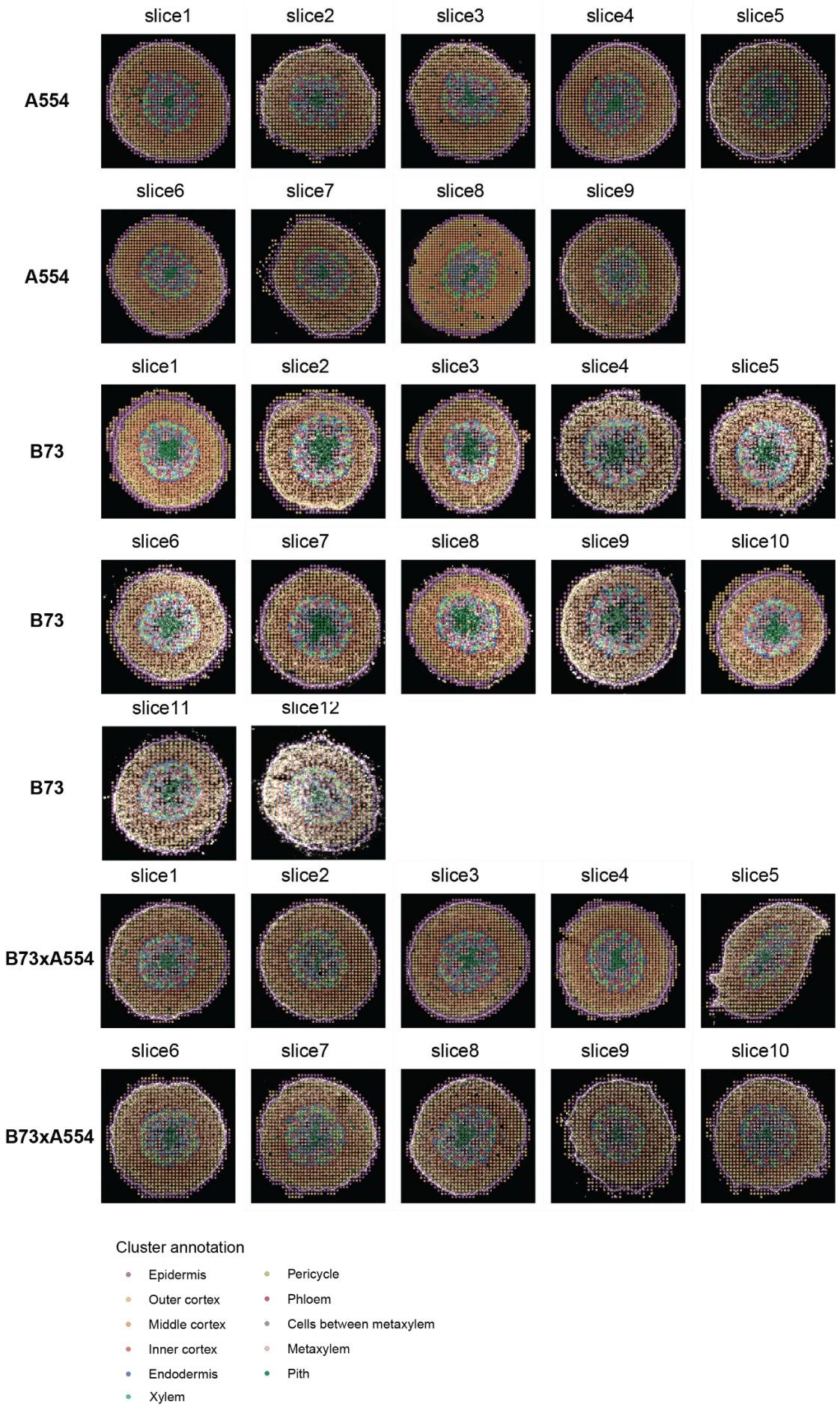



**Supplementary Figure S3. Quality control and filtering of the spatial transcriptomic dataset.** Quality-control assessment of spatial transcriptomic observations from maize roots of B73, A554, and B73 × A554. Violin plots (**a**) show the distributions of the number of detected genes (nFeature_Spatial) and total transcript counts (nCount_Spatial) for A554, B73, and the B73 × A554 hybrid. The scatter plot (**b**) shows the relationship between number of genes and total transcript counts for individual spatial spots, with points colored by genotype. The dashed horizontal line indicates the minimum number of genes threshold (n = 200) used for quality filtering.



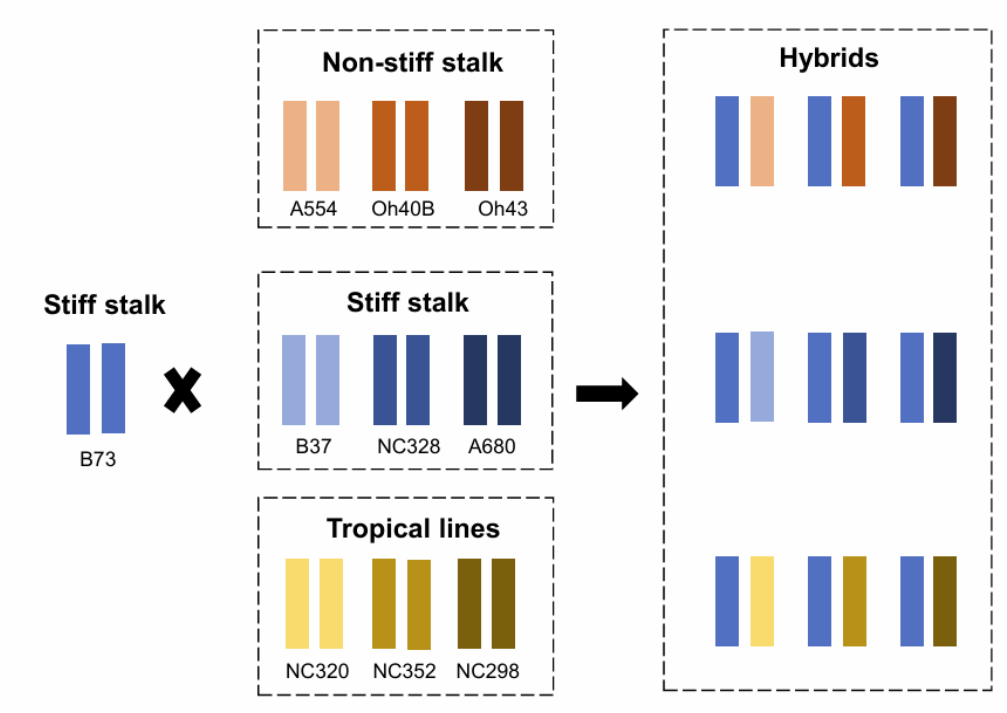

**Supplementary Figure S4. Cell-type annotation of root spatial transcriptome by selected marker genes.**

Dot plot showing the expression of selected marker genes across annotated root cell types in the spatial transcriptomic dataset. Dot size indicates the proportion of spatial spots expressing each gene, and dot color represents the average scaled expression level. Larger and more intensely colored dots therefore indicate stronger expression within the corresponding cell type. The plot was used to support and refine spatial cell-type annotation.


slice1
slice2
slice3
slice4
slice5
A554
slice6
slice7
slice8
slice9
A554
slice1
slice2
slice3
slice4
slice5
B73
slice6
slice7
slice8
slice9
slice10
B73
slice11
slice12
B73
slice1
slice2
slice3
slice4
slice5
B73xA554
slice6
slice7
slice8
slice9
slice10
B73xA554
Cluster annotation
Epidermis
Outer cortex
Middle cortex
Inner cortex
Endodermis
Xylem
Pericycle
Phloem
Cells between metaxylem
Metaxylem
Pith

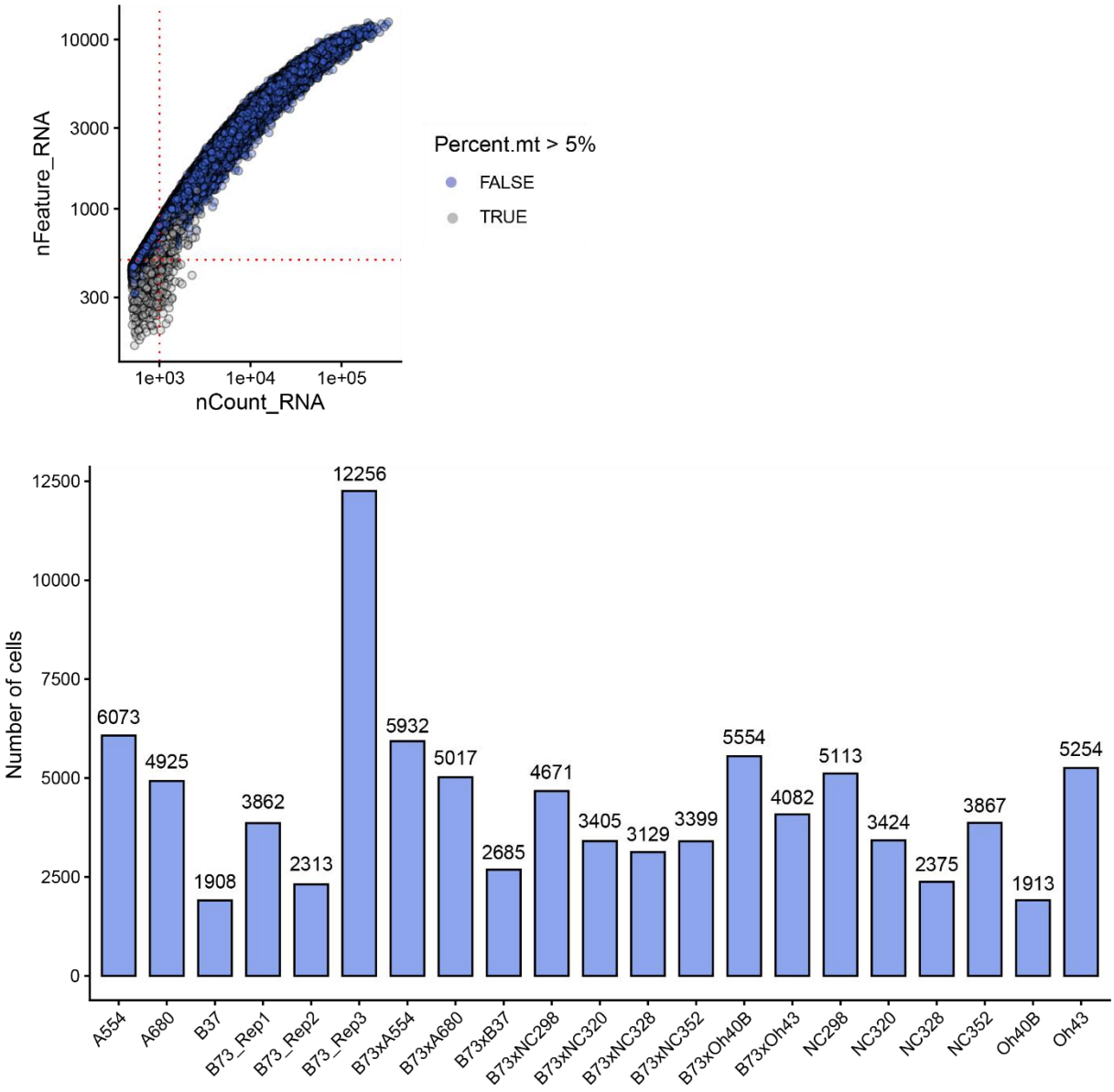
**Supplementary Figure S5. Spatial annotation of maize root cell types across 31 transverse sections from parental inbreds and their hybrid.**

Each panel represents an individual transverse section, with spatial spots colored according to assigned cell-type identity. Annotated cell populations include epidermis, outer cortex, middle cortex, inner cortex, endodermis, pericycle, phloem, xylem, cells between metaxylem, metaxylem, and pith. Serial sections illustrate the reproducibility of radial tissue organization across genotypes.




**Supplementary Figure 6. Genetic composition of the maize hybrid panel used for single-cell transcriptomic analyses.**

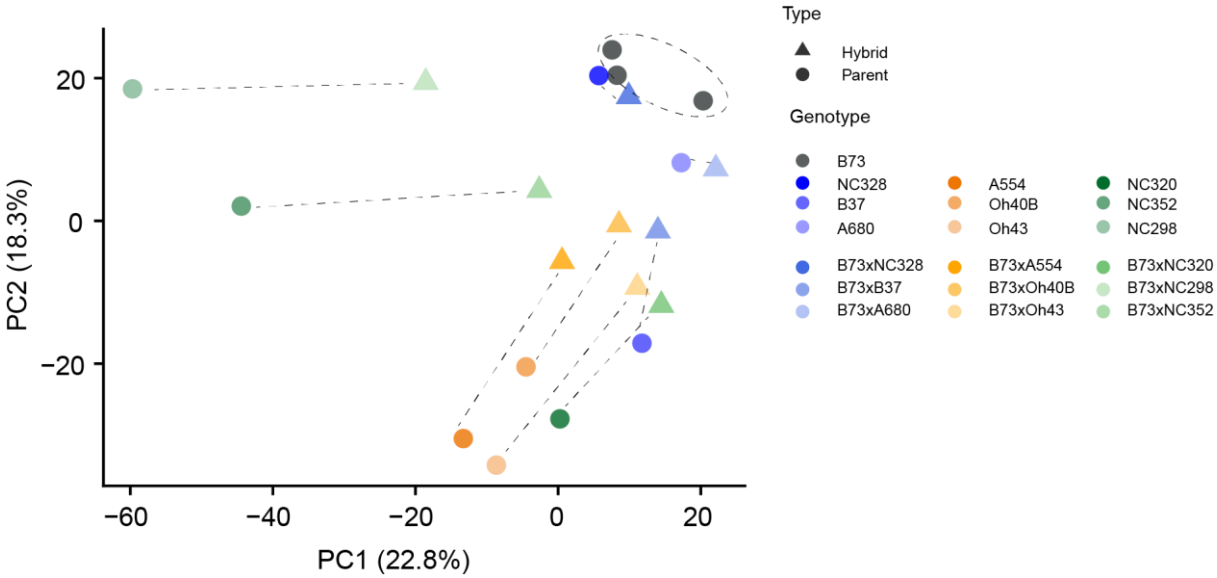
B73 was used as the common maternal parent and crossed with nine paternal inbred lines representing three genetic groups: non-stiff stalk (A554, Oh40B and Oh43), stiff stalk (B37, NC328 and A680), and tropical lines (NC320, NC352 and NC298). Coloured boxes denote the individual inbred lines, and the cross symbol indicates hybridization between B73 and each paternal line. Blue, orange and gold indicate stiff-stalk, non-stiff-stalk and tropical genetic backgrounds, respectively. The resulting nine B73-based $F_1$ hybrids were analysed together with their parental inbred lines.




**Supplementary Figure S7. Single-cell RNA-sequencing quality control, sample-level cell recovery, and replicate concordance in maize primary roots.**

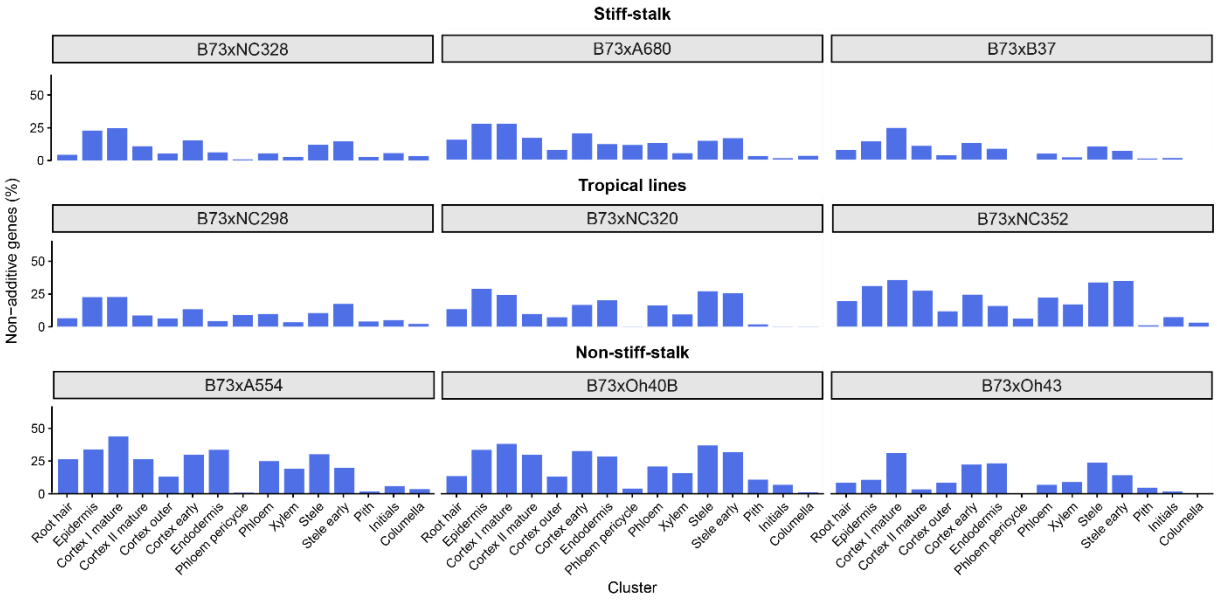
Single-cell transcriptomes were obtained from maize primary roots harvested 3 days after germination from 21 samples: three biological replicates of B73, nine paternal inbred lines, and the nine corresponding B73-based $F_1$ hybrids. (**a**) Cell-level quality-control plot showing total transcript counts (x-axis) versus the number of detected genes (y-axis); each point represents one cell. Colors indicate whether the mitochondrial transcript fraction exceeded 5% (TRUE, gray; FALSE, blue). Red dotted lines mark the thresholds used to filter cells with low transcript counts and/or few detected genes. Cells with more than 5% mitochondrial transcripts were also excluded. (**b**) Number of high-quality cells retained from each sample after filtering; numbers above the bars indicate sample-level counts. In total, 91,157 cells were retained for integrated analysis, clustering, cell-type annotation, and downstream analyses. (**c**) Heatmap of pairwise Spearman correlations in gene-expression profiles between the three B73 biological replicates (R1, R2, and R3), calculated separately for each annotated root cell type. Columns show the R1–R3, R1–R2, and R2–R3 comparisons, and rows represent cell types. Color encodes the

correlation coefficient, with warmer colors indicating higher and cooler colors lower correlations. Most cell types showed strong cross-replicate concordance, whereas Columella and Pericycle showed comparatively lower correlations.



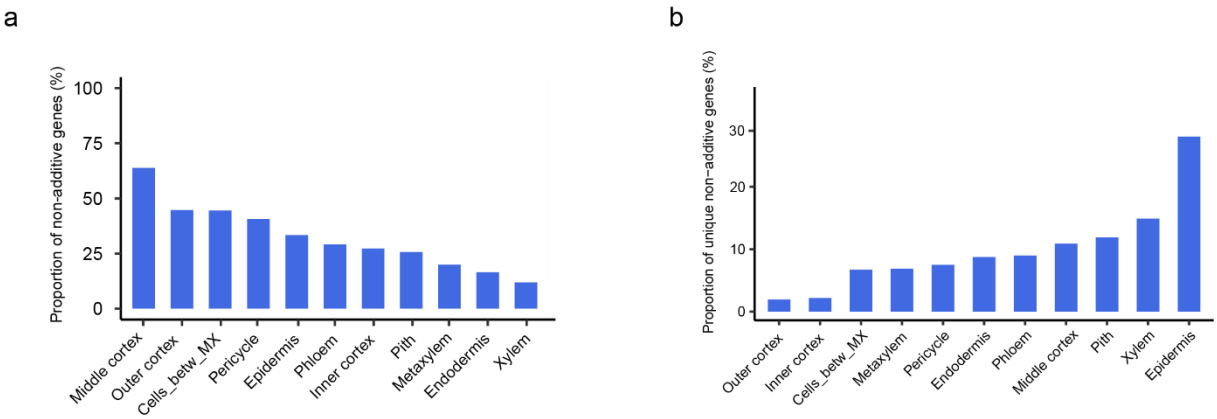

**Supplementary Figure S8. Pseudobulk principal component analysis of single-cell transcriptome samples.**

PCA based on sample-level pseudobulk gene-expression profiles generated by aggregating single-cell expression within each biological sample. PC1 and PC2 explain 22.8% and 18.3% of the total variance, respectively. Circles denote parental or replicate samples, and triangles denote B73-based hybrids. Colors indicate the genetic group of the non-B73 parent: B73 replicates (grey), stiff-stalk (blue), non-stiff-stalk (orange), and tropical backgrounds (green). Dashed lines connect each non-B73 parent with its corresponding hybrid. The dashed ellipse highlights the clustering of B73 biological replicates. The close grouping of B73 replicates, the separation of major paternal genetic backgrounds and the intermediate placement of many hybrids indicate reproducible sample-level relationships and contributions from both parental transcriptomes.



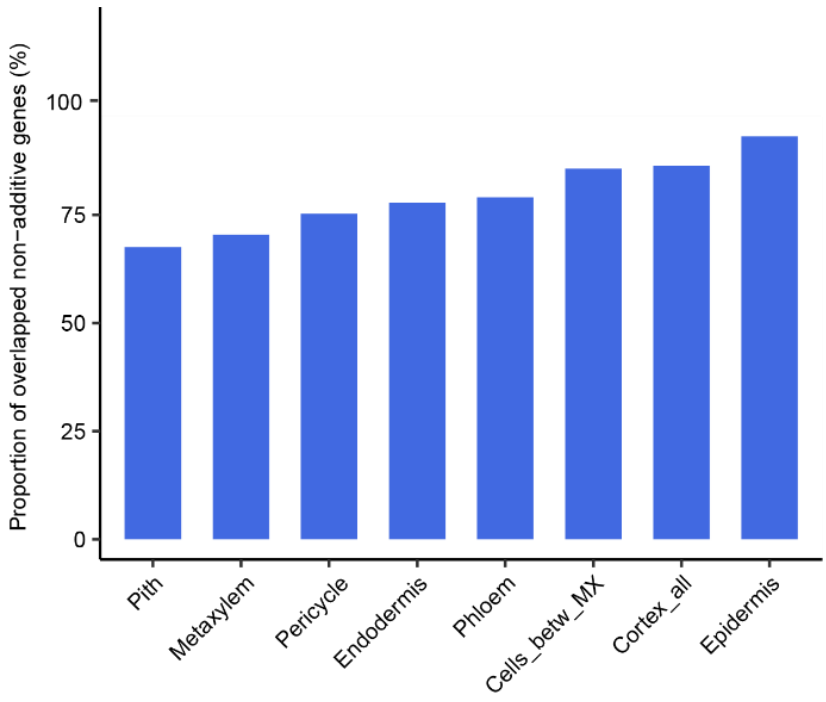

**Supplementary Figure S9. Percentage of non-additive genes across single-cell clusters for nine hybrid–parent triplets.**

Stacked bar plots show the proportion of expressed genes classified as additive or non-additive in each of the 15 single-cell clusters for nine B73-based hybrid–parent comparisons. Each facet represents one hybrid and its corresponding parental pair. For each cluster, blue segments indicate the percentage of genes exhibiting non-additive expression, whereas grey segments indicate additive expression; bars therefore sum to 100% within each cluster. Cluster numbers correspond to the integrated single-cell atlas described in Fig. 2. The extent of non-additive expression varied among hybrid combinations, with recurrent enrichment in clusters corresponding to cortex and epidermal populations.



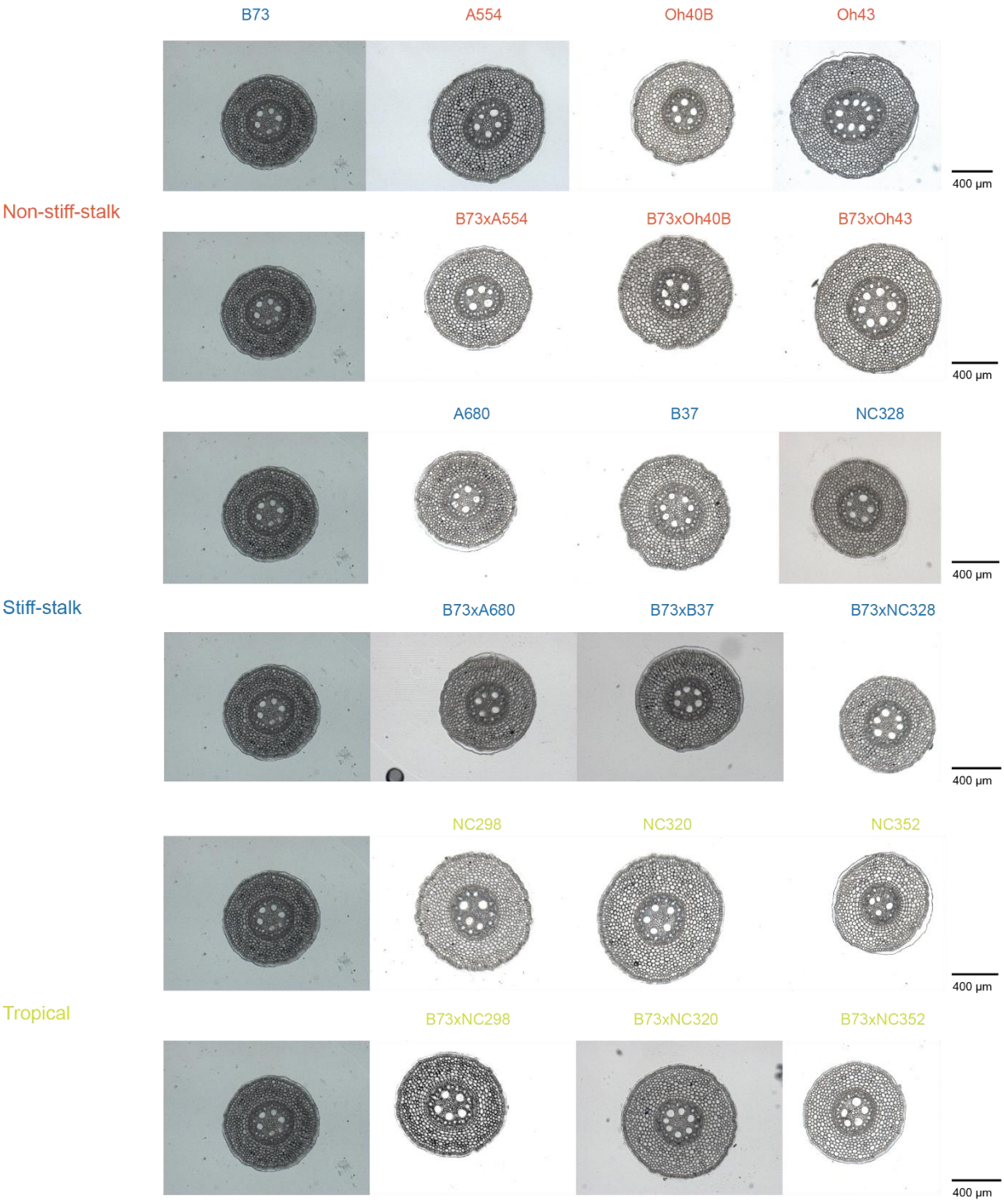

**Supplementary Figure S10. Spatial distribution and cluster specificity of non-additive genes.**

(**a**) Percentage of expressed genes classified as additive or non-additive across annotated spatial transcriptomic clusters in a hybrid–parent comparison. Each stacked bar represents one spatial cluster. Blue segments indicate the percentage of non-additive genes, whereas grey segments indicate the additive fraction; the two fractions sum to 100% within each cluster. (**b**) Percentage of cluster-specific non-additive genes across spatial transcriptomic clusters. Bars indicate the proportion of unique non-additive genes relative to the total number of non-additive genes detected in the corresponding cluster. Clusters are ordered according to their annotated spatial identities. The enrichment of unique non-additive genes in epidermal and xylem-associated clusters indicates that the spatial distribution of non-additive regulation combines shared transcriptional responses with cluster-specific components.



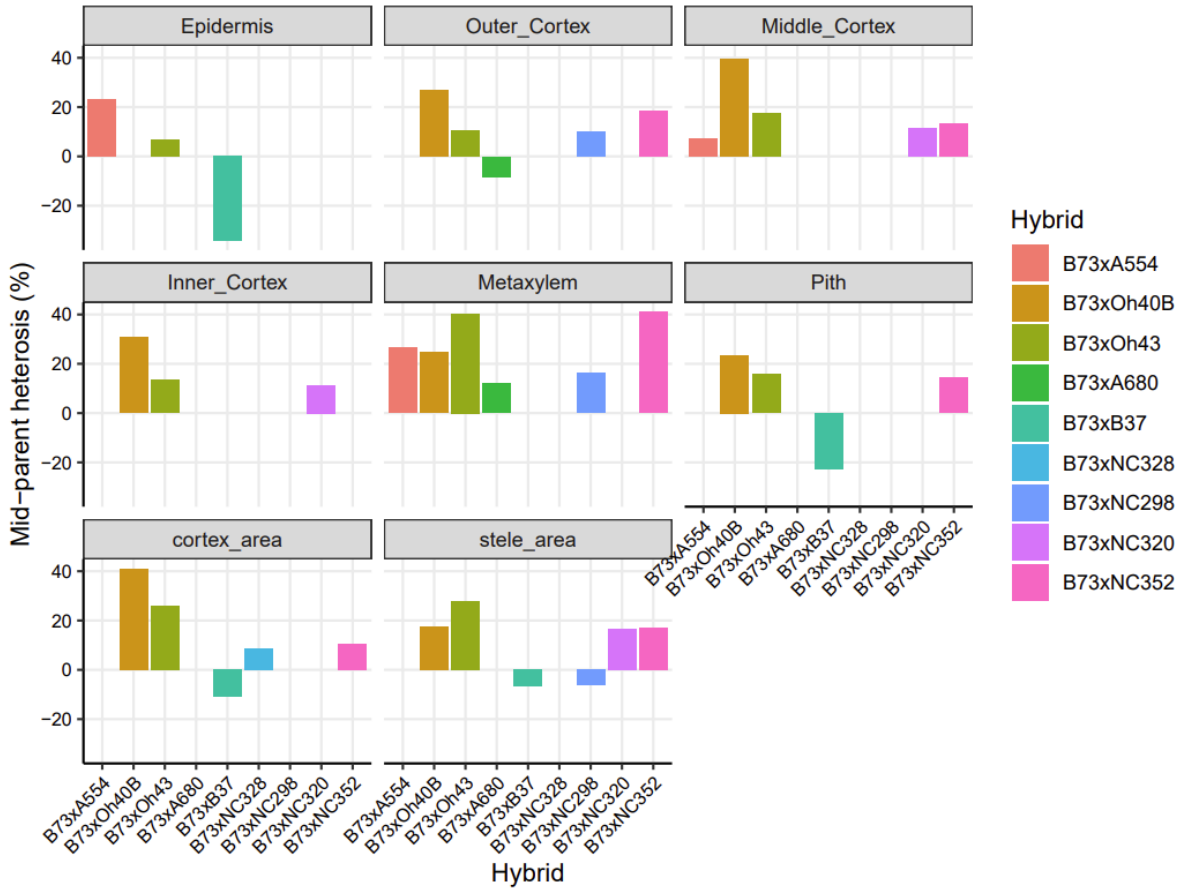

**Supplementary Figure S11. Overlap of non-additive genes identified by single-cell and spatial transcriptomics.**

Percentage of overlapping non-additive genes between the single-cell RNA-seq and spatial transcriptomic datasets across spatially annotated root clusters. Bars represent the proportion of non-additive genes shared between the two transcriptomic modalities for each cluster, calculated using the cluster-level overlap metric described in the Methods. Spatial clusters include pith, xylem-associated metaxylem cells, phloem-pole pericycle, endodermis, phloem, cells between metaxylem poles, the combined cortex population and epidermis. The highest overlap was observed in the epidermis and cortex, whereas pith and xylem-associated populations showed comparatively lower concordance.



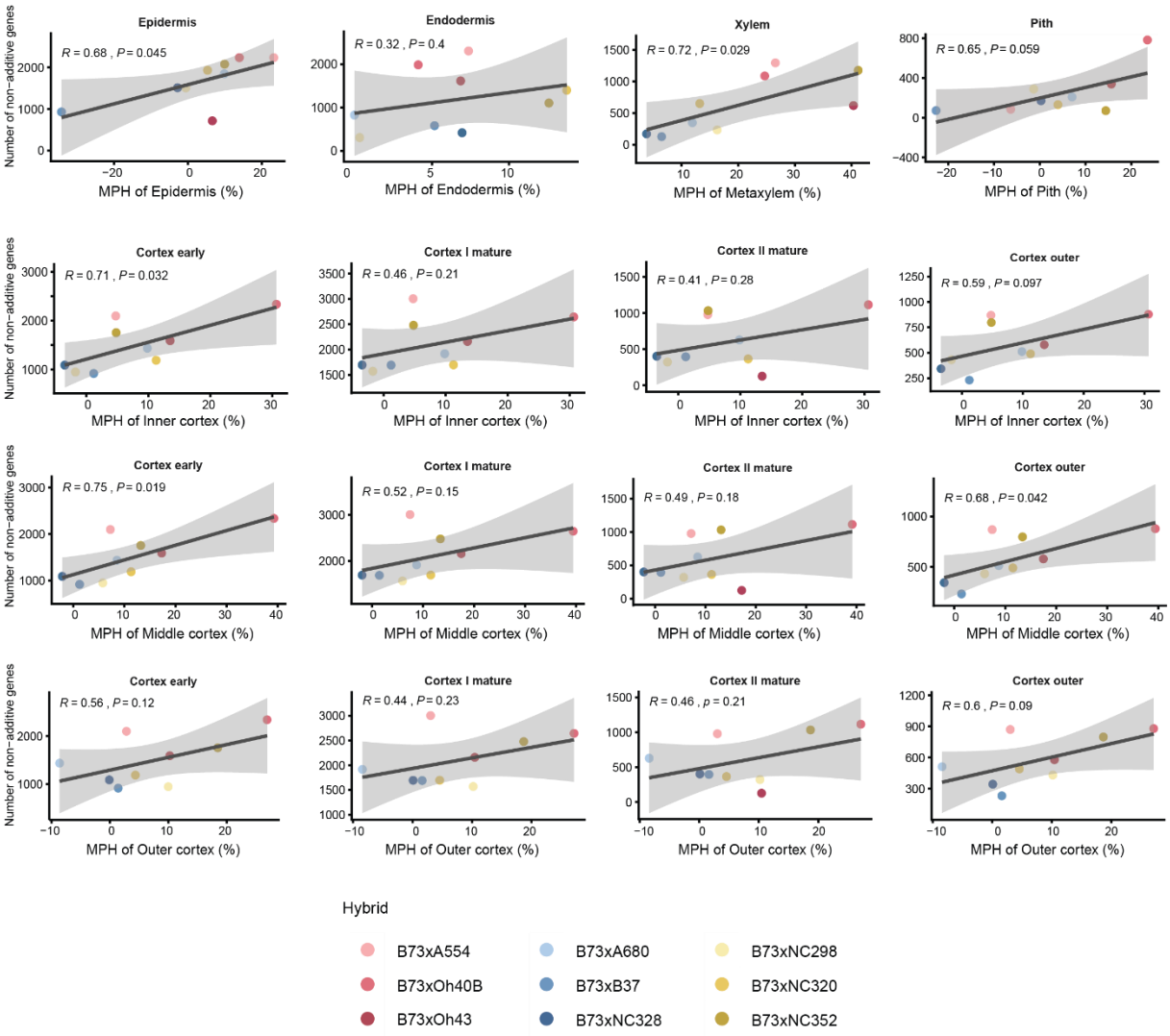

**Supplementary Figure S12. Root cross-sectional anatomy of maize inbred lines and their corresponding B73-derived hybrids representing distinct heterotic groups**.

Representative transverse root sections are shown for parental inbred lines and their corresponding hybrids. Genotypes are grouped into three categories: non-stiff-stalk, stiff-stalk, and tropical lines. For each parent-hybrid tripplet, mid-parent heterosis of cell size in epidermis, outer cortex, middle cortex, inner cortex, endodermis, metaxylem and pith were calculated, and overall cortex area, stele area.



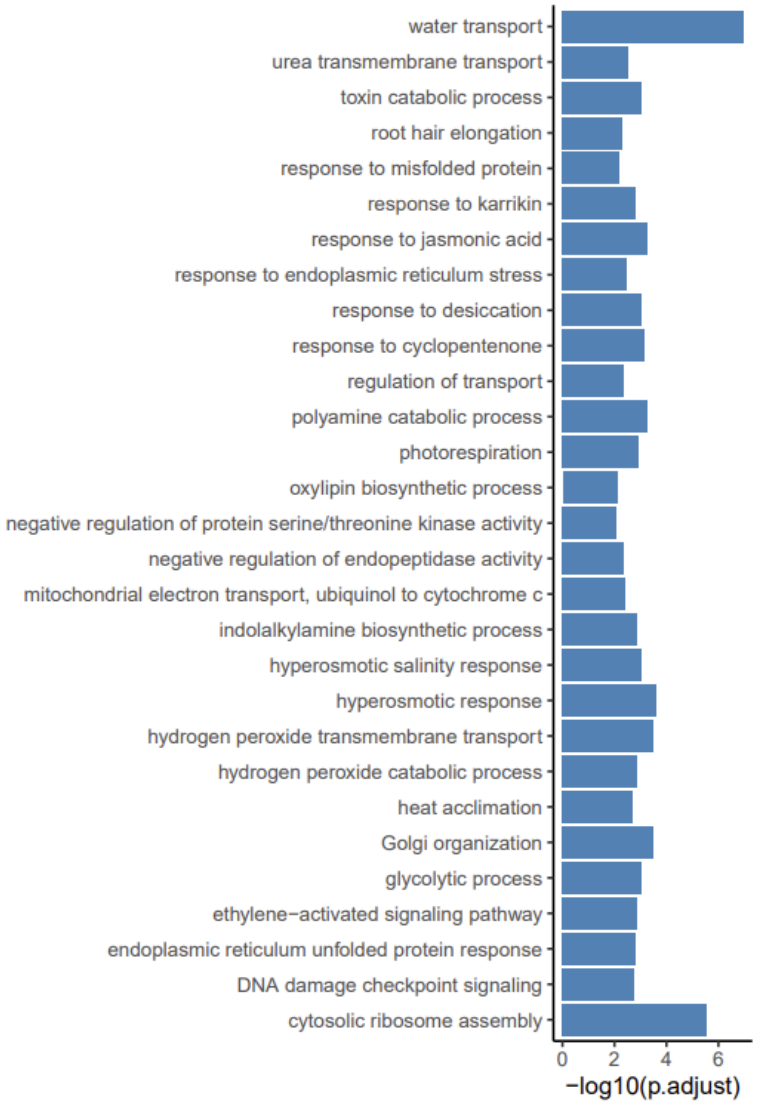

**Supplementary Figure S13. Mid-parent heterosis for root anatomical traits across hybrid–parent triplets.**

Faceted bar plots show the strength and direction of mid-parent heterosis (MPH) for anatomical traits measured in nine B73-based hybrid–parent triplets. Panels represent epidermal, outer-cortex, middle-cortex, inner-cortex, metaxylem and pith cell-size traits, together with cortex area and stele area. The x-axis shows the hybrid combinations, and the y-axis shows MPH expressed as a percentage. Positive values indicate that the hybrid exceeded the parental mean, whereas negative values indicate performance below the parental mean. Bar colors identify the hybrid combinations as indicated in the legend. Bars are shown only for traits and hybrid combinations with available measurements.



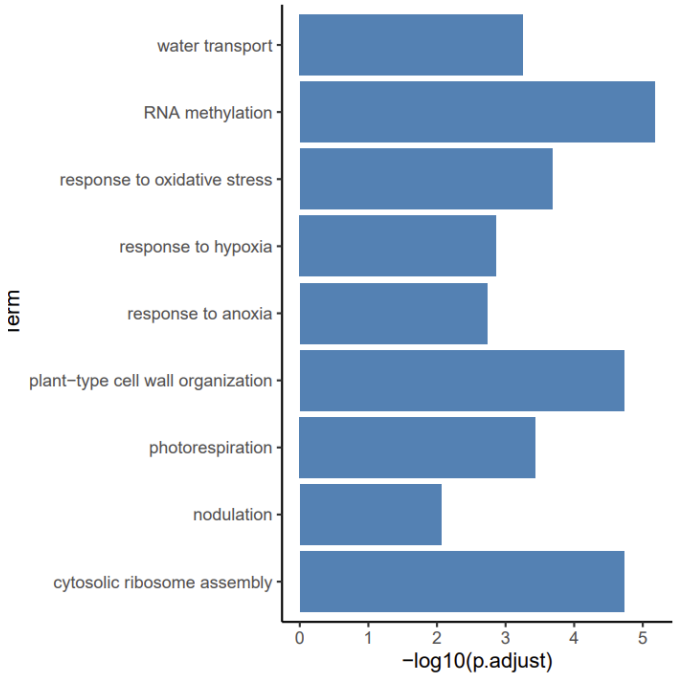

**Supplementary Figure S14. Associations between number of non-additive genes and cell-size heterosis**

Scatter plots showing the relationship between the number of non-additively expressed genes and mid-parent heterosis (MPH) for cell size across nine B73-based hybrids. Each point represents one hybrid, with colors indicating hybrid identity. The five panels show associations for epidermis cluster 1, middle-cortex cluster 0, middle-cortex cluster 4, middle-cortex cluster 9 and metaxylem cluster 10, respectively. The x-axis shows cell-size MPH, and the y-axis shows the number of non-additive genes detected in the corresponding single-cell cluster. The black line represents the fitted linear regression, and the grey band indicates the 95% confidence interval. The reported correlation coefficient (*R*) and *P* value are shown in each panel.



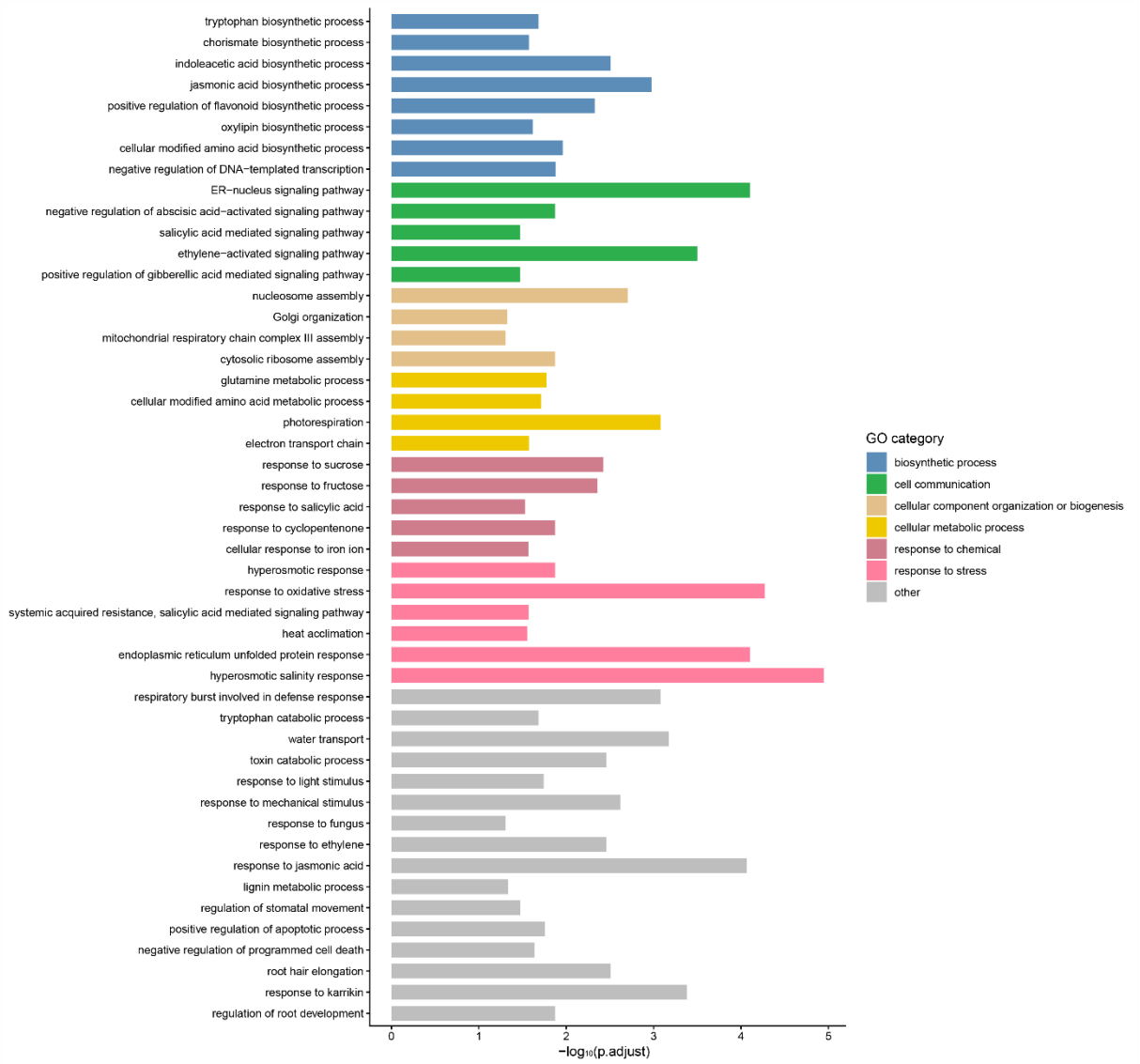

**Supplementary Figure S15. Gene Ontology enrichment of recurrent non-additive genes in cortex cluster 0.**

Gene Ontology biological-process enrichment among non-additively expressed genes detected in cortex cluster 0 in at least seven hybrid combinations. Horizontal bars show enriched terms, and bar length represents enrichment significance as $-\log_{10}(P\text{adjusted})$. Recurrent cortex non-additive genes were associated with water and urea transport, regulation of transport, root-hair elongation, jasmonate-, ethylene- and karrikin-responsive processes, oxylipin and polyamine metabolism, osmotic and salinity responses, heat acclimation, peroxide metabolism, and endoplasmic-reticulum and protein-stress responses. These enrichments indicate that recurrent cortex regulation involves transport capacity, developmental growth and adaptation to environmental stress.

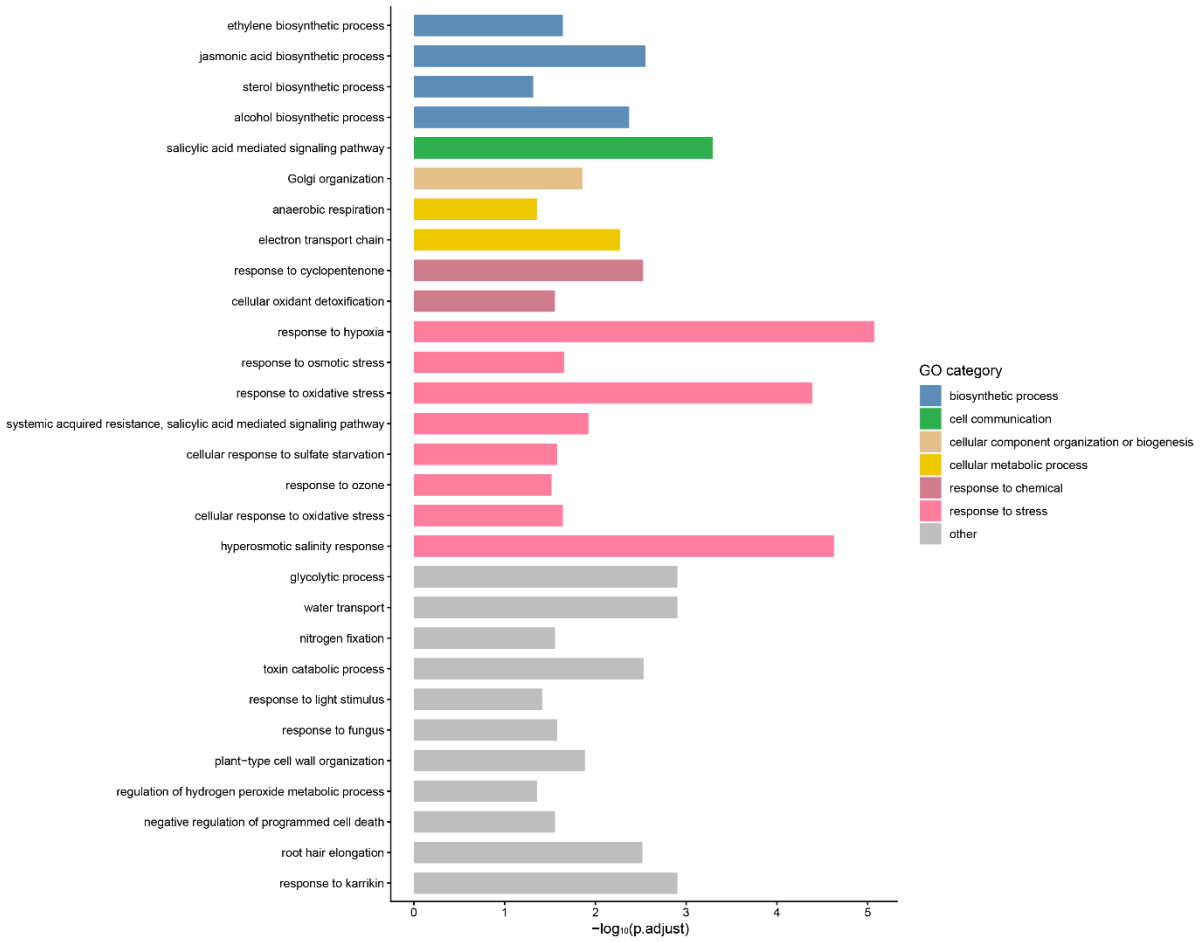



**Supplementary Figure S16. Gene Ontology enrichment of recurrent non-additive genes in epidermis cluster 1.**

Gene Ontology biological-process enrichment among non-additively expressed genes detected in epidermis cluster 1 in at least seven hybrid combinations. Horizontal bars show enriched terms, and bar length represents enrichment significance as $-\log_{10}$ (*P* adjusted). Enriched processes included water transport, plant-type cell-wall organization, responses to oxidative stress, hypoxia and anoxia, photorespiration, RNA methylation, nodulation-associated processes and cytosolic ribosome assembly. These terms indicate that recurrent epidermal non-additive regulation is linked to water movement, cell-wall organization, stress adaptation, translational capacity and interactions with the root environment.

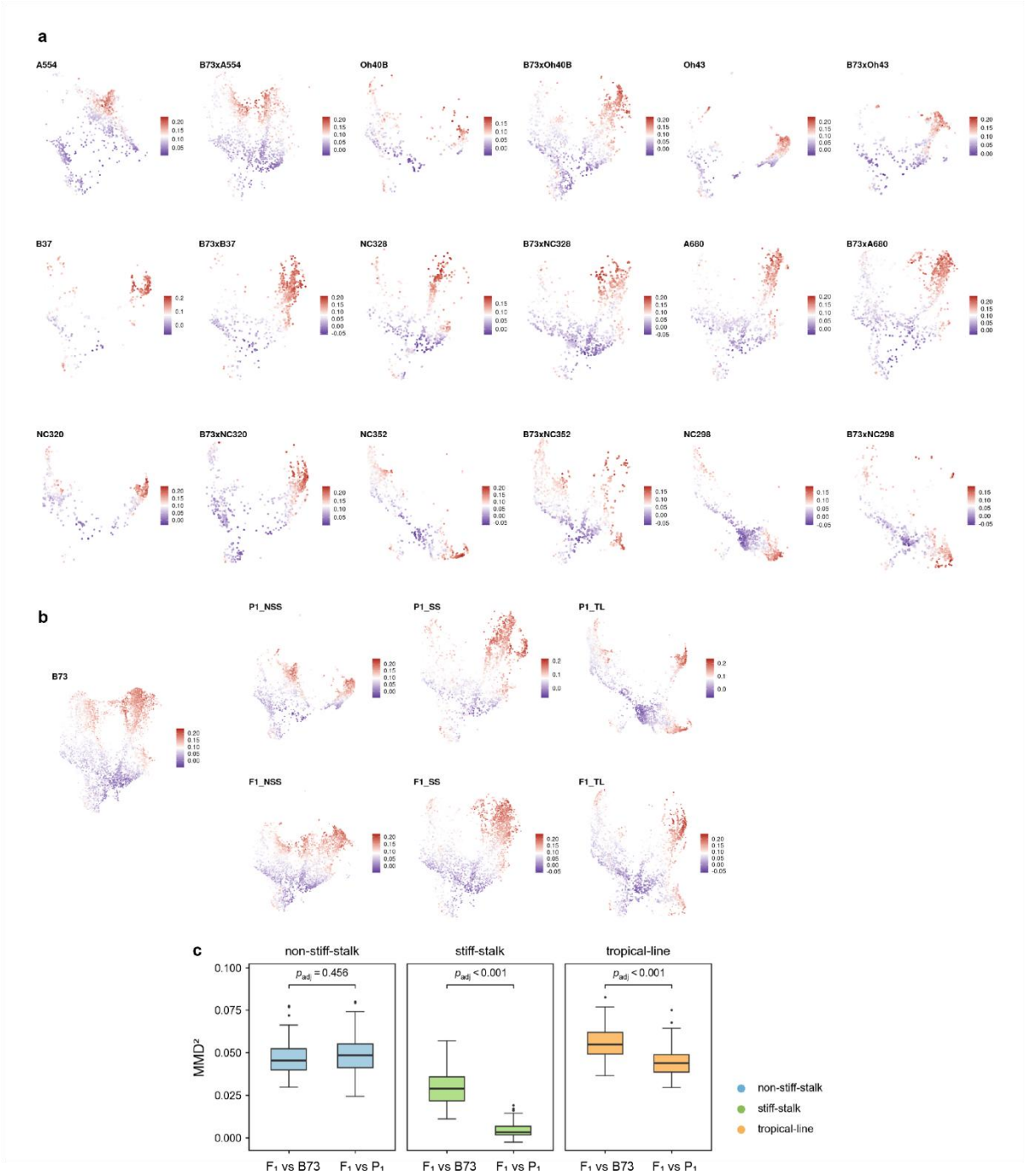



**Supplementary Figure S17.** Level-4 Gene Ontology enrichment of cortex genes shared between non-additive and cross-specific expression sets. Barplot of enriched Gene Ontology biological-process terms among genes that were both non-additively expressed in the B73 × Oh40B cortex and differentially expressed between B73 × Oh40B and B73 × A554 cortex tissues. Enriched terms are organized around broader level-4 functional categories. The barplot highlights cellular processes related to biosynthetic process, cell communication, metabolic process and response to stress.




**Supplementary Figure S18. Level-4 Gene Ontology enrichment of epidermal genes shared between non-additive and cross-specific expression sets.**

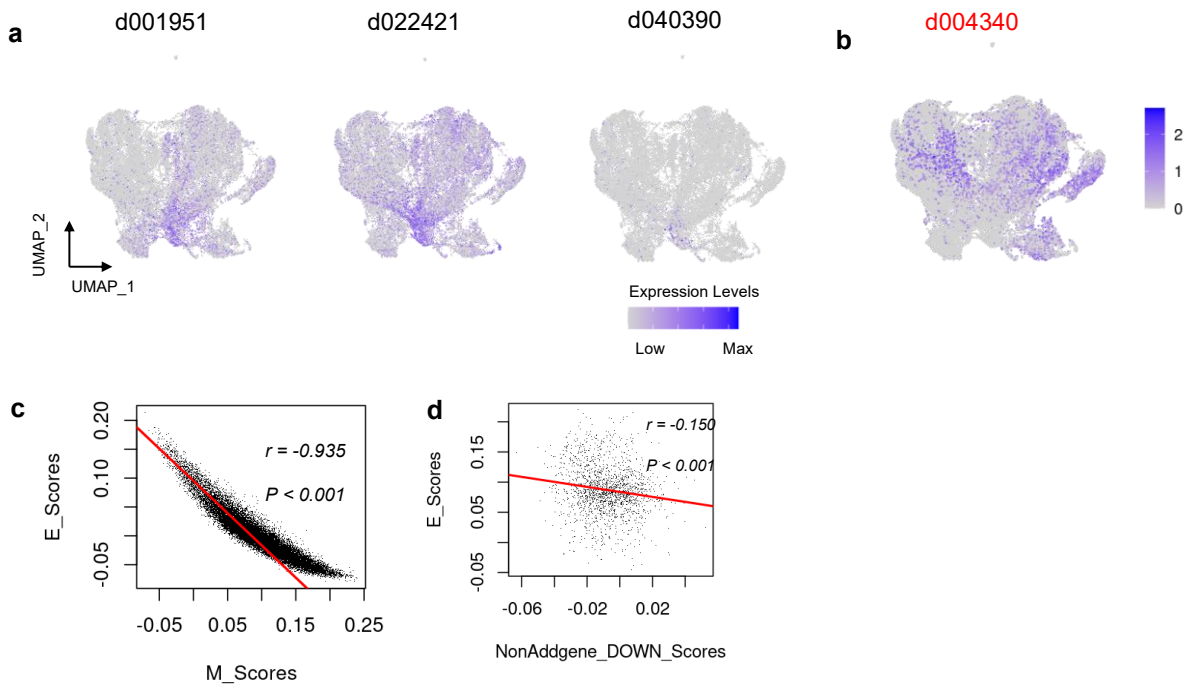
Barplot of enriched Gene Ontology biological-process terms among genes that were both non-additively expressed in the B73 × A554 epidermis and differentially expressed between B73 × A554 and B73 × Oh40B epidermal tissues. Enriched terms are organized around broader level-4 functional categories. The barplot highlights cellular processes related to cell wall organization and root-hair and developmental regulation, and responses to abiotic and biotic stresses, including oxidative stress, hypoxia, salinity, ozone, fungal stimuli and chemical stress.




**Supplementary Figure S19 Genotype-dependent cortex developmental states and parental transcriptomic affinities.**

**a,** Cortex cells from nine paternal inbred lines and their corresponding B73-based $F_1$ hybrids displayed on a common UMAP embedding. **b,** Cortex cell distributions for B73 and pooled non-B73 parents (P1) and hybrids ($F_1$), grouped as non-stiff-stalk (NSS), stiff-stalk (SS) or tropical-line (TL). In **a** and **b**, each point represents one cell coloured by the elongation-associated developmental score (E_Score), with purple and red indicating lower and higher scores, respectively. Colour scales are shown separately for each panel. **c,** Squared maximum mean discrepancy (MMD²) between pooled $F_1$ cortex transcriptomes and B73 or the corresponding P1 pool, calculated in a shared expression space; lower values indicate greater distributional similarity. Boxes summarize 100 paired resampling iterations, each sampling 100 cells per population with replacement. Centre lines indicate medians; box limits indicate the first and third quartiles; whiskers extend to the most extreme values within 1.5 times the interquartile range;

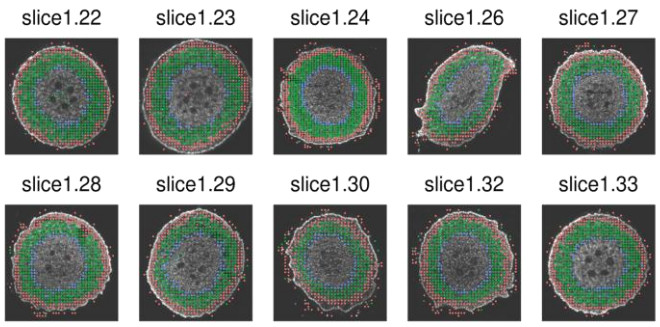
points indicate outliers. Adjusted *P* values were obtained from two-sided relative-MMD tests using 2,000 held-out cells per population, with Bonferroni correction across the three groups (NSS, *P*adj = 0.456; SS, *P*adj = $1.09 \times 10^{-25}$; TL, *P*adj = $2.95 \times 10^{-5}$).



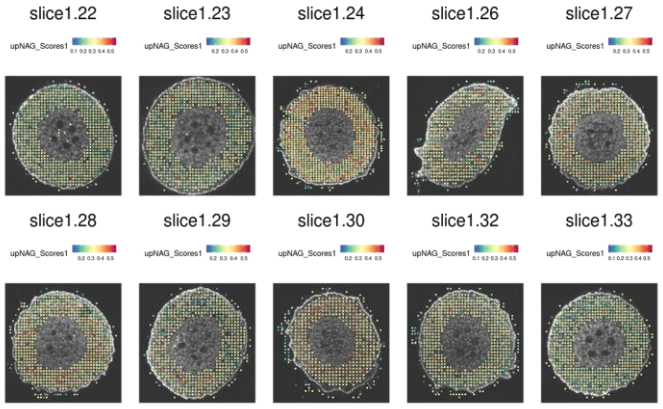

**Supplementary Fig. S20 Gene-expression patterns and developmental score associations in maize cortex cells.**

**a**, UMAP expression maps of *Zm00001d001951*, *Zm00001d022421* and *Zm00001d040390*, associated with early developmental states. **b**, Expression of the elongation-associated gene *Zm00001d004340* in later cortex states. Grey-to-purple colours indicate increasing expression. **c**, Strong inverse association between meristematic (M_Score) and elongation-associated (E_Score) scores ($r = -0.935$, $P < 0.001$). **d**, Weak negative association between E_Score and the module score for non-additive genes with negative mid-parent heterosis in B73×Oh40B cortex cells ($r = -0.150$, $P < 0.001$). Each point represents one cell. Red lines indicate least-squares linear fits; correlation coefficients and two-sided *P* values were calculated using Pearson's correlation test.

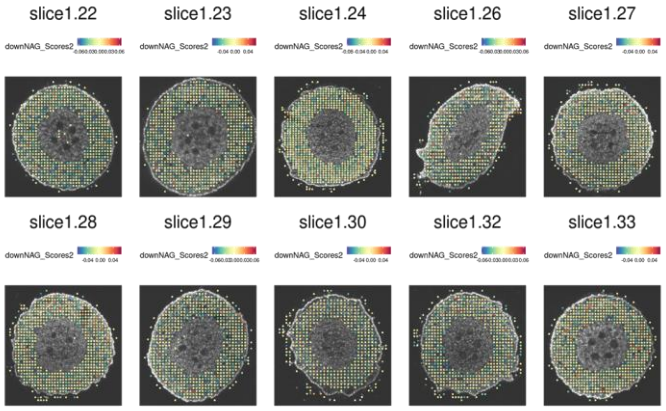
a


slice1.22
slice1.23
slice1.24
slice1.26
slice1.27
slice1.28
slice1.29
slice1.30
slice1.32
slice1.33

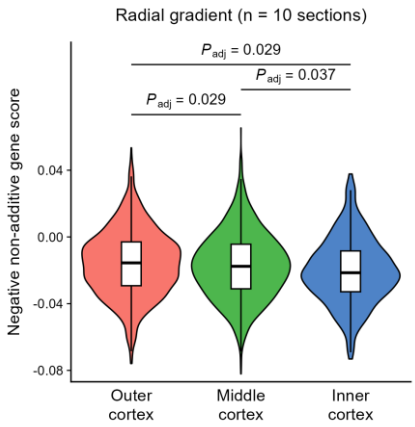
b


slice1.22
slice1.23
slice1.24
slice1.26
slice1.27
slice1.28
slice1.29
slice1.30
slice1.32
slice1.33

c

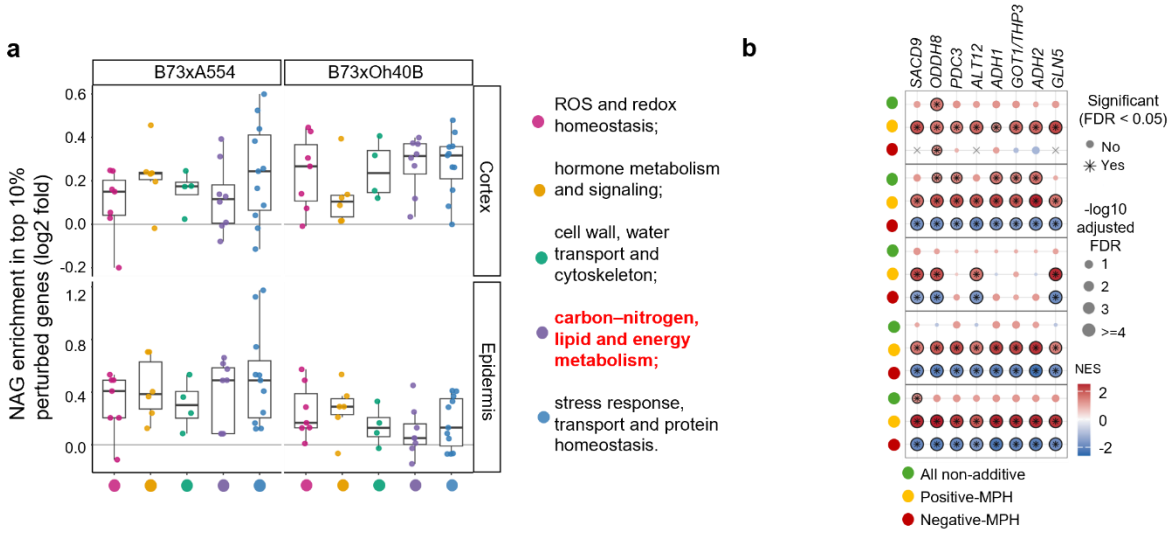

slice1.22
slice1.23
slice1.24
slice1.26
slice1.27
slice1.28
slice1.29
slice1.30
slice1.32
slice1.33

d


Radial gradient (n = 10 sections)
$P_{adj}$ = 0.029
$P_{adj}$ = 0.037
$P_{adj}$ = 0.029
Negative non-additive gene score
0.04
0.00
-0.04
-0.08
Outer cortex
Middle cortex
Inner cortex

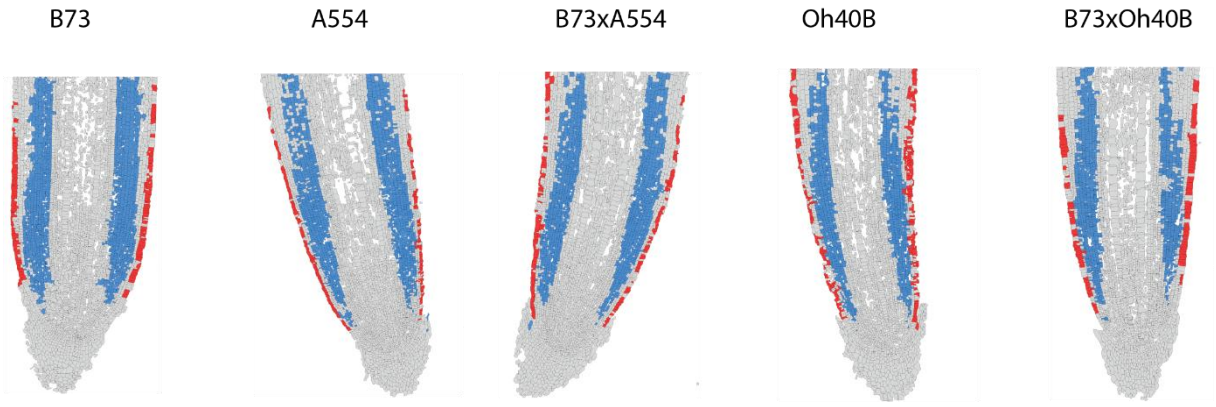
**Supplementary Figure S21. Spatial distribution of non-additive gene expression across cortex layers.**

**a**, Spatial annotation of outer (red), middle (green; Cortex) and inner (blue) cortex in ten A554×B73 root sections. **b**, Spatial distribution of module scores for non-additive genes with positive mid-parent heterosis. **c**, Spatial distribution of module scores for non-additive genes with negative mid-parent heterosis, with an accompanying violin plot showing their radial variation (d). Each point in the spatial maps represents a spatial bin; colour bars indicate module scores. Violins show pooled bin-level distributions across the ten sections. White boxes indicate medians and interquartile ranges; whiskers extend to the most extreme values within 1.5× the interquartile range. Pairwise comparisons used two-sided paired Wilcoxon signed-rank tests on within-section layer medians ($n$ = 10 sections), with Benjamini–Hochberg adjustment across the three comparisons. Adjusted $P$ values are shown.



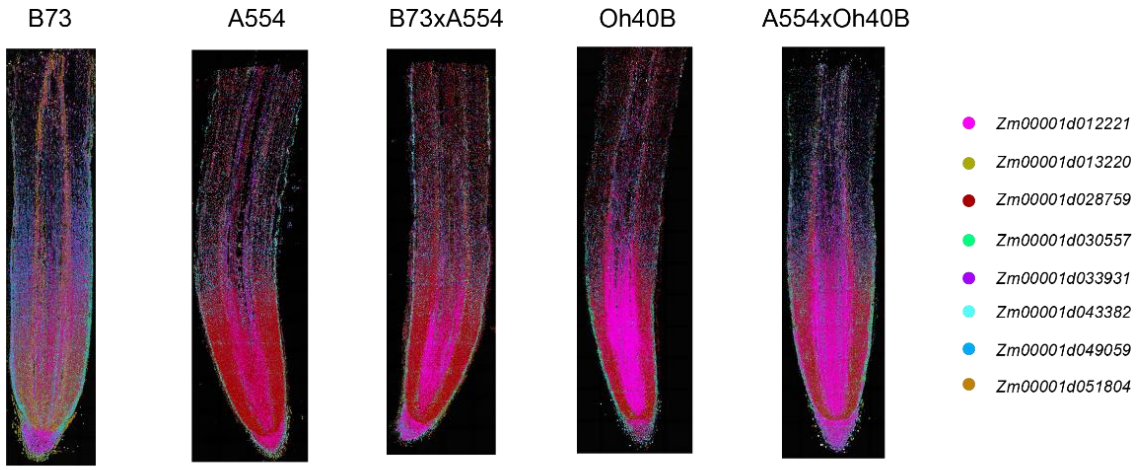

**Supplementary Figure S22. Tissue-specific non-additive gene perturbations and positive-MPH enrichment associated with carbon–nitrogen metabolism.**

**a,** NAG enrichment among the top 10% of perturbed genes across five functional modules. Points represent Knock Out genes; boxes show medians and interquartile ranges. **b,** GSEA of all, positive-MPH, and negative-MPH NAGs. Color indicates NES, size indicates $-\log_{10}$FDR, and asterisks denote FDR < 0.05.




**Supplementary Figure S23. Multiplex FISH localization of cortex and epidermis marker genes**

Multiplex fluorescence *in situ* hybridization (FISH) was performed on longitudinal root sections from B73, A554, Oh40B and the corresponding hybrids B73 × A554 and B73 × Oh40B. Each panel shows the merged spatial signals of cortex marker gene (*Zm00001d019565*) and epidermis marker gene (*Zm00001d037547*) analyzed in that genotype, with red represent epidermal marker and blue represent cortical marker.




**Supplementary Figure S24. Multiplex FISH localization of heterosis-associated candidate genes**

Multiplex fluorescence *in situ* hybridization (FISH) was performed on longitudinal root sections from B73, A554, Oh40B and the corresponding hybrids B73 × A554 and B73 × Oh40B. Each panel shows the merged spatial signals of the candidate genes analyzed in that genotype, with the detected gene IDs listed alongside the root image. The longitudinal sections encompass the root tip and successive developmental zones, allowing assessment of gene localization along the root axis. Many candidate genes showed preferential or enriched expression in cortex-associated regions, providing anatomical validation of the transcriptomic cell-type assignments and enabling comparison of spatial expression patterns across parental and hybrid genotypes.